Zhang, Fan; Cannone Falchetto, Augusto; Wang, Di; Li, Zhenkun; Sun, Yuxuan; Lin, Weiwei

Prediction of asphalt rheological properties for paving and maintenance assistance using explainable machine learning

Published in:
Fuel

DOI:
10.1016/j.fuel.2025.135319

Published: 15/09/2025

Document Version
Publisher's PDF, also known as Version of record

Fuel 396 (2025) 135319

Contents lists available at ScienceDirect

Fuel

journal homepage: www.elsevier.com/locate/fuel

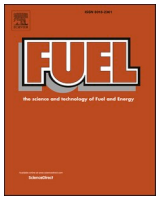

Full Length Article

Prediction of asphalt rheological properties for paving and maintenance assistance using explainable machine learning

Fan Zhang [a], Augusto Cannone Falchetto [a,b], Di Wang [a,c], Zhenkun Li [a,*], Yuxuan Sun [a], Weiwei Lin [a]

[a] Department of Civil Engineering, Aalto University, Rakentajanaukio 4, 02150 Espoo, Finland
[b] Department of Civil Environmental and Architectural Engineering, University of Padova, Via Marzolo 9, 35131 Padova, Italy
[c] Department of Civil Engineering, University of Ottawa, 800 King Edward Ave, Ottawa, ON K1N 6N5, Canada

ARTICLE INFO

Keywords:
Asphalt binders
Rheological properties
Chemical composition
Explainable machine learning
SHAP

ABSTRACT

Conventional frequency-temperature sweep tests for evaluating asphalt rheological properties are time-consuming and resource-intensive. The characterization efficiency can be significantly improved by establishing a robust predictive model that links rheological properties to chemical composition. To this end, this study investigates the correlation between asphalt's chemical and rheological properties and develops precise predictive models using machine learning techniques. The input features include eleven key functional groups measured by Fourier Transform Infrared Spectroscopy (FTIR), while the output variables are the complex modulus ($|G^*|$) and phase angle (δ) from Dynamic Shear Rheometer (DSR). Five machine learning algorithms—multiple linear regression, support vector regression, artificial neural network, random forest, and eXtreme gradient boosting (XGBoost)—were utilized to construct the predictive models. A Bayesian optimization strategy was employed to fine-tune their hyperparameters. Laboratory findings revealed that a strong correlation was identified between changes in these functional groups, especially oxygen-containing functional groups, and the $|G^*|$ and δ values of asphalt binders. The optimized XGBoost model achieved exceptional predictive accuracy, with R^2 values of 0.9998 for $|G^*|$ and 0.9999 for δ. Additionally, SHapley Additive exPlanations (SHAP) values were used to elucidate the underlying principles of the predictions. By leveraging FTIR data and rheological indicators, this work provides a novel data-driven approach to accurately estimate asphalt binder behaviour, reducing experimental effort while ensuring reliable performance evaluation.

1. Introduction

Asphalt properties such as adhesion, rheology, fatigue, etc. are critical to the life of the pavement [1,2]. Rheological properties, among them, determine the deformation behaviour of asphalt binders and directly affect the overall performance of the pavement. The rheological properties of asphalt binders reflect their viscoelastic characteristics and exhibit different mechanical behaviours at different temperatures and loading conditions [3,4]. Changes in these properties are closely linked to pavement distress such as rutting, fatigue, and cracking [5–7]. For instance, rutting is more likely to occur at high temperatures when the viscous component of the binder dominates. Therefore, understanding rheological properties is essential for preventing pavement distress and extending the service life of asphalt pavements. By adjusting the composition, modification technology and optimising the material ratio, the rheological properties of asphalt can be improved and its adaptability under different environmental conditions can be enhanced.

Testing of asphalt rheological properties, however, is usually time-consuming, with full-temperature and full-frequency tests usually taking several days to complete. For this reason, researchers have attempted to analyze the factors affecting rheological properties, such as chemical composition, to generate the model. Studies have demonstrated a strong correlation between the rheological properties of asphalt and its chemical composition [8–10]. Efforts have been made to analyze asphalt composition to predict rheological properties. For example, Sultana and Bhasin found that there is a strong relationship between the stiffness and strength of binders and their components, and these properties increase with the polar fractions [11]. Similarly, Cao et al. and Zhang et al. observed that the change in the asphalt's composition due to the addition of polymers can result in better

* Corresponding author.
E-mail address: zhenkun.li@aalto.fi (Z. Li).

https://doi.org/10.1016/j.fuel.2025.135319
Received 4 March 2025; Received in revised form 24 March 2025; Accepted 4 April 2025
Available online 10 April 2025

properties at both high and low temperatures [3,12]. Michalica et al. predicted the rheological properties at high and low temperatures as well as the oxidative aging process by analyzing the composition of bitumen from different sources [13]. These studies provide a theoretical basis for rapid characterization of asphalt rheological properties.

Despite these findings, current research has limitations: (1) There is insufficient exploration of the relationship between chemical functional groups and the rheological properties. While four-component and elemental analyses provide initial insights into rheological properties, these methods are often time-consuming. Establishing a correlation between functional group information from Fourier transform infrared spectroscopy (FTIR) and rheological properties could significantly reduce testing time and improve efficiency. (2) Existing studies primarily establish qualitative relationships between asphalt's micro-composition and rheological properties, lacking quantitative accuracy. This limits the decision-maker's ability to make precise adjustments without relying on trial-and-error methods. Additionally, these models often consider only single effects and fail to account for the nonlinear relationships inherent in materials, while small sample datasets further reduce prediction accuracy.

Recent advancements in machine learning have enabled its application in structural health monitoring, material characterization, performance prediction, and distress detection for civil infrastructure [14–18]. Machine learning models can address these limitations by handling multi-dimensional and complex data with higher accuracy than traditional models [19–22]. For instance, Hosseini et al. predicted the modulus and phase angle of different modified binders at low and medium temperatures using various machine-learning algorithms [23]. Similarly, Ziari et al. accurately predicted the rutting performance of asphalt binders modified by carbon nanotubes using neural networks and regression models [24]. Arifuzzaman et al. [25] and Tarefder et al. [26] successfully predicted the adhesion properties of bitumen by neural networks with the combination of laboratory characterization. These studies highlight machine learning as a powerful tool for developing predictive models for asphalt binder performance.

Based on the above literature review, a strong correlation between rheological properties and the chemical composition of bitumen can be identified, while machine learning algorithms are considered to be a powerful and accurate tool for predicting models. Hence, this study aims to establish predictive models linking the rheological properties of asphalt binders to their chemical composition using machine learning techniques. Asphalt samples with varying parameters (oil source, batch, grade, aging level, and bio-extender content) were collected. Rheological properties and chemical composition were measured using a Dynamic Shear Rheometer (DSR) and FTIR tests, respectively. A preliminary analysis of the relationship between rheological properties and chemical composition was conducted. Subsequently, an eXtreme Gradient Boosting (XGBoost) model was developed, and four other common models were tested for comparison. Finally, the contributions of input features were interpreted to provide insights into the model's predictions.

2. Materials and methods

Considering the effects of different sources, batches, penetrations, aging levels, and extenders, a total of 67 asphalt samples were collected (Details of these samples are summarized in Appendix). Short-term aging was achieved using the Rolling Thin Film Oven Test [27], while long-term aging was conducted using the Pressure Aging Vessel (PAV) test [28]. Extended long-term aging involved prolonged PAV testing (2PAV: 40 h, 3PAV: 60 h, 4PAV: 80 h, 5PAV: 100 h).

2.1. Fourier transform infrared (FTIR) spectroscopy test

The FTIR tests were conducted via a Nicolet iS50 machine. The asphalt binders were first heated to a soft state and a small amount of binders was deposited into the testing paper. Before each measurement, the system was background-corrected using an empty ATR crystal, and then the diamond crystals were gently pressed onto the sample with nine replicates over a wavenumber range of 600 cm^{-1} to 4000 cm^{-1}, with 32 scans per sample. After measurement, the spectra were baseline corrected and smoothed by OMNIC software to obtain the final FTIR spectra, as shown in Fig. 1.

The presence of various functional groups and chemical bonds in asphalt molecules results in distinct vibrational frequencies, which correspond to specific infrared absorption bands [29,30]. From Figs. 1 and 11 typical absorbance peaks can be identified, each corresponding to specific wavenumbers and vibrational modes [31–33]. Although some functional groups exhibit absorption peaks between 3000 cm^{-1} and 4000 cm^{-1}, their variations across samples are minimal, and thus, they were not considered as features in this study [34]. It is common to evaluate chemical changes of binders by absorption peak area, which are effective in distinguishing between different binder samples and have been chosen to feature [31]. They are labelled in subsequent content as A + wavenumber, e.g. A1700 means the absorption peak area of the binder at 1700 cm^{-1} wavenumber.

2.2. Dynamic Shear Rheometer tests

The rheological properties of asphalt binders were assessed using a Dynamic Shear Rheometer (DSR). The testing protocol included a temperature-frequency (*T-f*) sweep [35] conducted at low, medium, and high-temperature levels using three different parallel plate fixtures. The testing process and parallel plate configurations are illustrated in Fig. 2. Detailed testing parameters and fixture sizes are provided in Table 1.

The rheological properties of asphalt binders are characterized by the complex shear modulus ($|G^*|$) and phase angle (δ), which serve as the output variables in this study. Master curves were employed to explore the relationship from laboratory results based on the time–temperature superposition principle [36], as illustrated in Fig. 3. Various master curve models [3,37,38] have been developed based on this theoretical framework, and the model in this study was selected based on the Willams-Landel-Ferry model [39] due to its strong theoretical foundation in describing the temperature dependence of viscoelastic materials.

3. Machine learning theories

Multiple linear regression (MLR) [40] and Support Vector Machine (SVM) [41] have been widely used for regression and classification tasks. SVM can handle both linear and nonlinear relationships between inputs and outputs, achieving high accuracy and robustness even with complex datasets. Artificial neural networks (ANN) [42] is another powerful tool, which typically owns an input layer, several hidden layers, and an output layer, as shown in Fig. 4. Neurons are interconnected across layers, with weights determining the influence of one neuron on another. Random forest (RF) [43] is a fundamental ensemble learning method, in which multiple decision trees are constructed during training. Every tree will be trained using a random subset of the dataset, reducing overfitting and improving predictive performance. eXtreme gradient boosting (XGBoost) [44,45] is a commonly used ensemble learning algorithm, offering an efficient implementation of gradient boosting. It sequentially enhances each subsequent model using gradient descent and incorporates regularization techniques (l_1 and l_2) to penalize overfitting.

Although the aforementioned models are powerful, their performance depends on selecting appropriate hyperparameters. To maximize predictive accuracy, this study employs Bayesian optimization to determine optimal hyperparameters for all models except MLR [46]. Bayesian optimization uses a Gaussian Process as a surrogate model. Unlike traditional methods that rely on preset combinations, it dynamically evaluates previously tested combinations to select the next set of

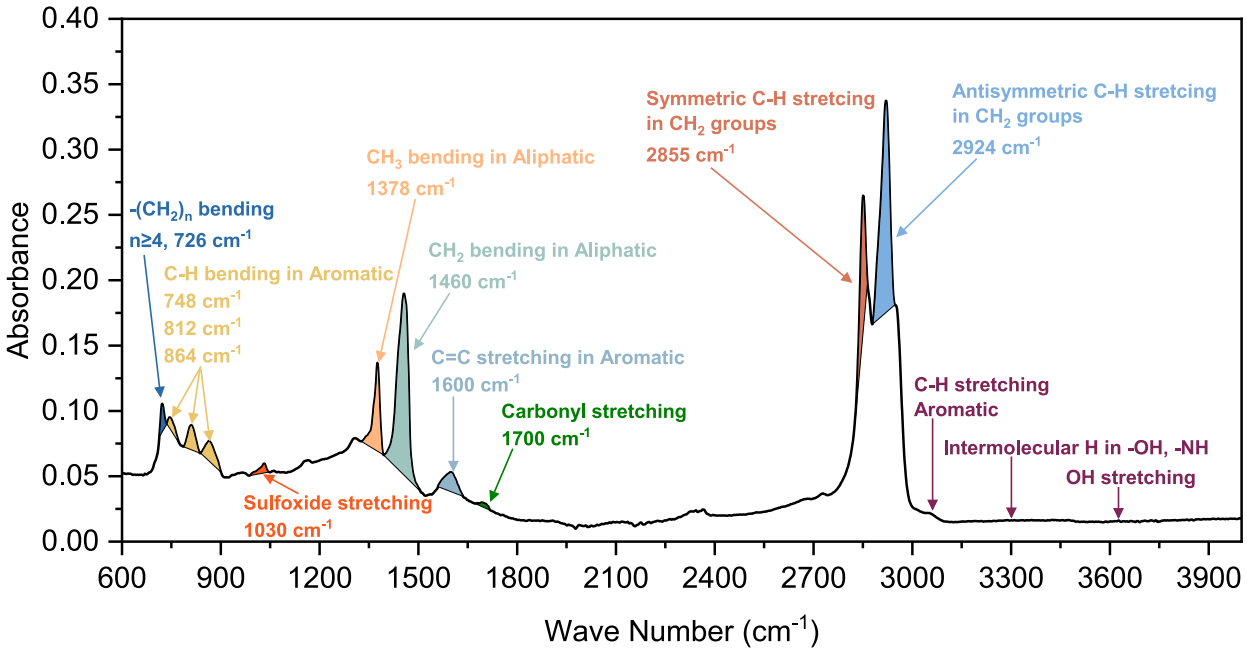

Fig. 1. FTIR description of asphalt binder.

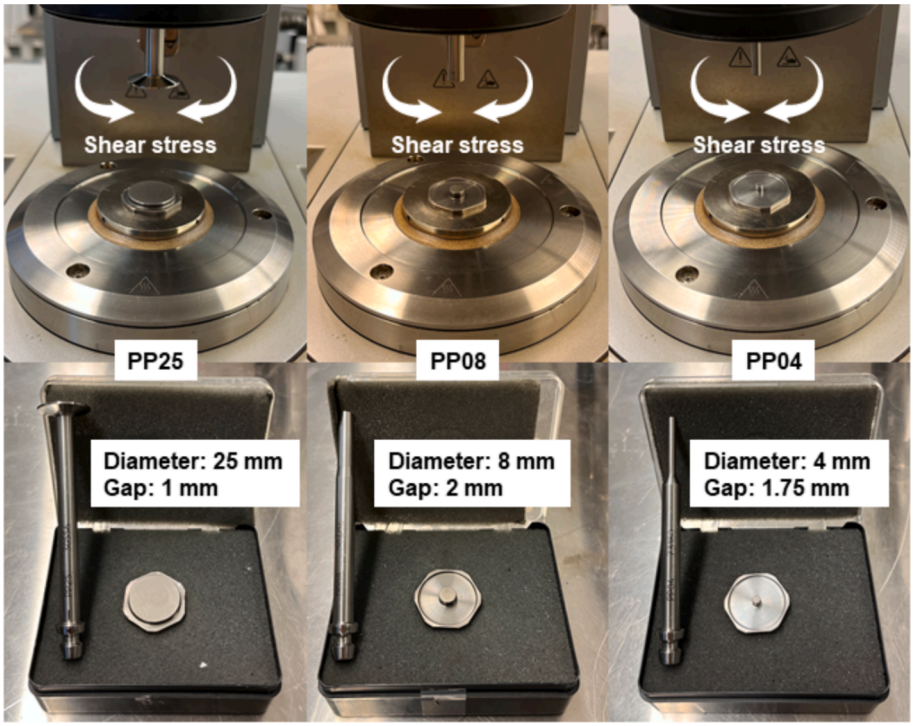

Fig. 2. DSR parallel plates.

parameters. By sampling a fixed number of hyperparameters from predefined distributions, it efficiently identifies the optimal combination.

4. Results and discussion

4.1. Correlation exploration based on laboratory data

The FTIR and DSR results of bitumen samples with different effects are presented in Figs. 5–7. It can be observed that the FTIR spectra in Fig. 5(a) are very similar, indicating that the chemical compositions of binders with different sources are nearly identical. Similarly, their master curves for $|G^*|$ (Fig. 6(a)) and δ (Fig. 7 (a)) are closely aligned, suggesting that they exhibit comparable rheological properties. Based on the laboratory results, no clear relationship between the chemical composition and rheological properties of asphalt from different oil sources is evident, necessitating further analysis using machine learning tools. A sensitivity analysis of different chemical components to the oil source can be quantified using the weight values (W_i) [47,48] in Table 2 (Equations are in the Appendix). All functional groups exhibit varying sensitivity to oil sources, with the group around 1030 cm^{-1} being the

Table 1
Details of DSR tests.

Experimental information	Values		
Temperature range	High temperatures	Mid temperatures	Low temperatures
Temperature/°C	34, 40, 46, 52, 58, 64, 70, 76, 82	−6, 0, 4, 10, 16, 22, 285, 34, 40	−30, −24, −18, −12, −6, 0, 4
Frequency/Hz	0.1, 0.2, 0.3, 0.4, 0.5, 0.6, 0.7, 0.8, 0.9, 1.0, 1.59, 2, 3, 4, 5, 6, 7, 8, 9, 10	0.1, 0.2, 0.3, 0.4, 0.5, 0.6, 0.7, 0.8, 0.9, 1.0, 1.59, 2, 3, 4, 5, 6, 7, 8, 9, 10	0.1, 0.2, 0.3, 0.4, 0.5, 0.6, 0.7, 0.8, 0.9, 1.0, 1.59, 2, 3, 4, 5, 6, 7, 8, 9, 10
Linear viscoelastic range/%	1	0.1	0.05
Fixture diameter/mm	25	8	4
Fixture gap/mm	1	2	1.75

most sensitive. Since the asphalt samples are not aged and therefore no absorption peak is formed due to the oxidation reaction [49,50], the stretching vibrations of C=O around 1700 cm^{-1} do not appear, resulting in no significant fluctuations across different oil sources.

Variations in production batches of asphalt binders can lead to minor differences in binder properties due to inconsistencies in production processes. Three asphalt samples, identical except for their batch, were selected, and their FTIR and DSR results are shown in Figs. 5(b), 6(b), and 7(b). It can be observed that their FTIR spectra overlap almost entirely, making it difficult to distinguish between batches based on FTIR results alone. Similarly, their master curves, particularly for the $|G^*|$, also overlap significantly. This indicates that laboratory results alone cannot establish a preliminary relationship between the rheological properties of asphalt binders and their chemical composition. The W_i of samples from different batches is similar to the effect of oil sources, the functional groups exhibit low sensitivity to production batches, with a maximum weight value of 20.18 %.

The FTIR spectra and master curves of samples with different penetrations are presented in Figs. 5(c), 6(c), and 7(c). The FTIR spectra of the samples show a trend of overlapping lines, indicating similar chemical compositions, but the peak areas vary slightly due to differences in the vibrational strengths of the functional groups. From master curves, a clear pattern in the rheological properties of the samples is evident: the $|G^*|$ decreases as the penetration grade increases, while the δ increases. The S=O stretching vibrations around 1030 cm^{-1} are the most sensitive to penetration grade, with a weight value exceeding 44 % in Table 2. This suggests that the S=O stretching vibrations significantly influence the rheological properties of asphalt binders.

The FTIR spectra and master curves of samples with different aging levels are shown in Figs. 5(d), 6(d), and 7(d). Significant variations are observed in the spectra, particularly in the S=O stretching vibrations (1030 cm^{-1}) and C=O stretching vibrations (1700 cm^{-1}). The W_i for these two functional groups exceeds 80 %. Specifically, the band area of sulfoxide stretching increases with higher aging levels, especially after PAV aging. Additionally, the FTIR spectra at 1700 cm^{-1} reveal a new carbonyl absorption peak, indicating that the asphalt has undergone oxidation [51]. These changes in chemical composition lead to variations in rheological properties. The master curves of $|G^*|$ and δ shift upward and downward, respectively, as the aging level of the asphalt binders increases. This suggests that the increase in the intensity and area of sulfoxide stretching, along with the presence of carbonyl groups, results in an increase in the elastic component and a decrease in the viscous component of the asphalt.

The FTIR spectra and DSR results of neat binders and bio-extended binders are shown in Figs. 5(e), 6(e), and 7(e). The primary differences between these samples are observed in the C-O-C stretching vibrations of oxygen-containing functional groups [52,53] (e.g., esters), as well as the carbonyl vibrations around 1700 cm^{-1} in the FTIR spectra. The addition of bio-extenders increases the intensity and area of these functional groups, resulting in a high W_i above 68.3 %. The enhancement of these functional group vibrations leads to a decrease in the $|G^*|$ and an increase in the δ, causing the asphalt to exhibit a more viscous component.

Laboratory results show that the chemical information of samples is consistent with that in Fig. 1, mainly caused by vibrations of C-H, C=O, C=C, S=O, and C-O-C. For fresh binders, their lack of oxidation reaction makes the C=O located in 1700 cm^{-1} of their FTIR spectra equal to 0 [49]. These fresh binders can be distinguished from different sources by S=O vibrations at 1030 cm^{-1} and from different batches of the same

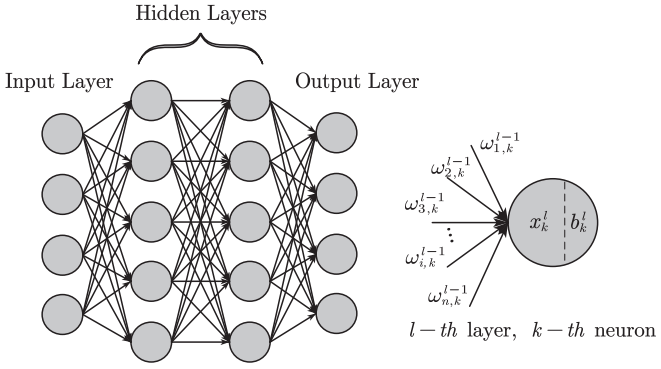

Fig. 4. Illustration of an ANN.

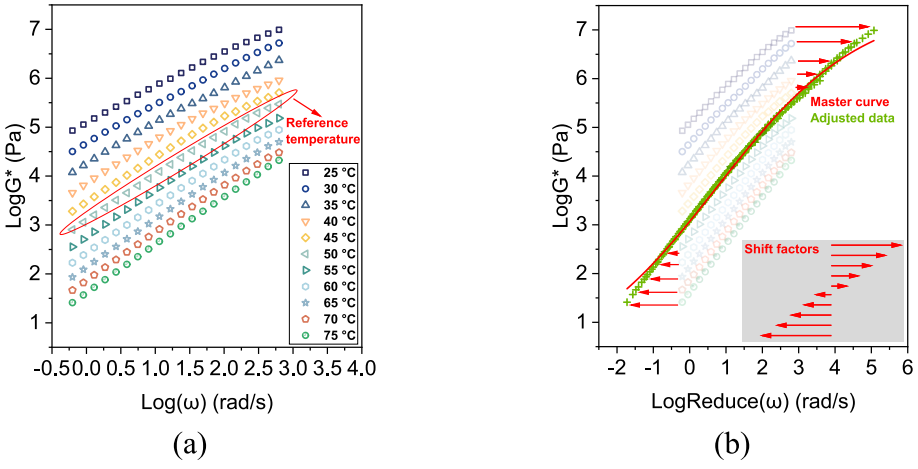

Fig. 3. Example of master curves.

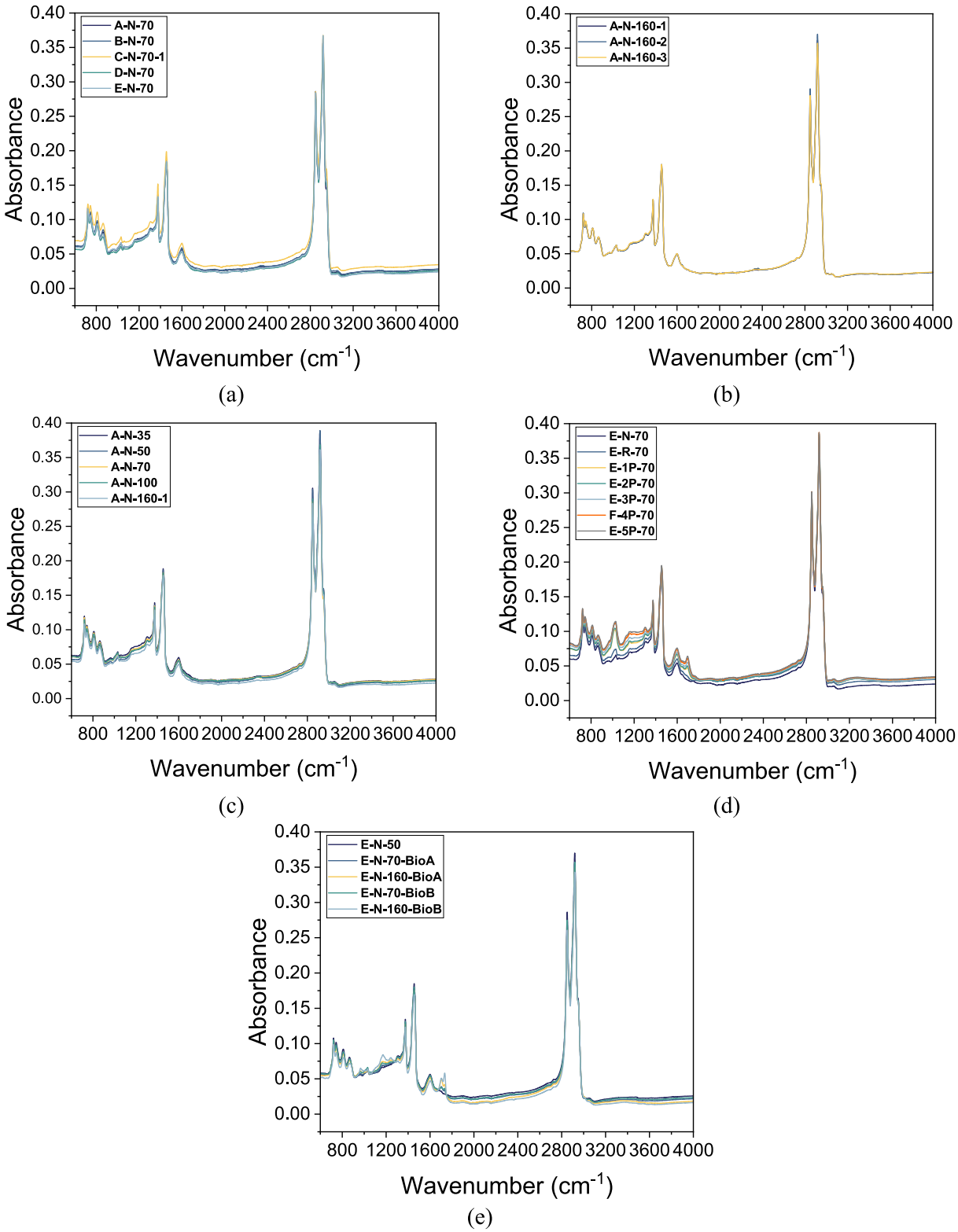

Fig. 5. FTIR results of binders with different effects: (a) source; (b) batch; (c) penetration; (d) aging; (e) extender.

source by C-H vibrations at 864 cm^{-1}. This is because different sources and production processes result in various sulphur contents in binders, resulting in a large variation in the absorption peak at 1030 cm^{-1}. Similarly, since the binder with higher penetration has more light components while the low-penetration binder contains more gums and asphaltenes [54], this makes the polar components such as sulphur-containing functional groups more variable, causing them to be significantly different at 1030 cm^{-1}. Ageing is due to oxidation reactions that cause the binder to form new oxygen-containing functional groups and change the sulphur content and chemical structure [55]. As a result, oxygen combines with carbon and sulphur in the bitumen to form C=O and S=O, which greatly increases the absorption peaks at 1700 cm^{-1} and 1030 cm^{-1} and deepens with aging. The biomaterials themselves contain a high amount of C=O functional groups, which makes the bio-

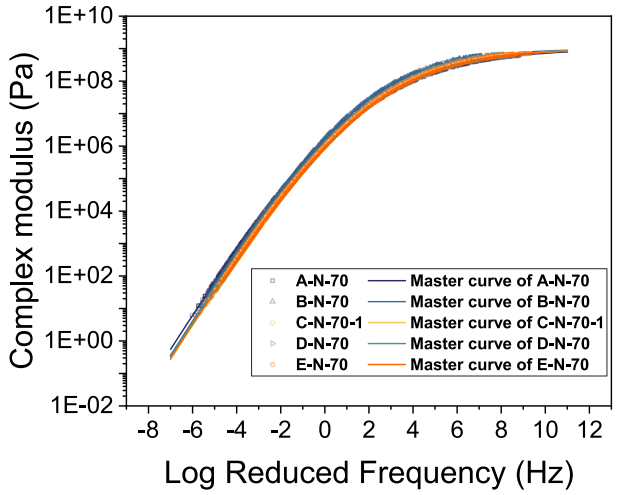

(a)

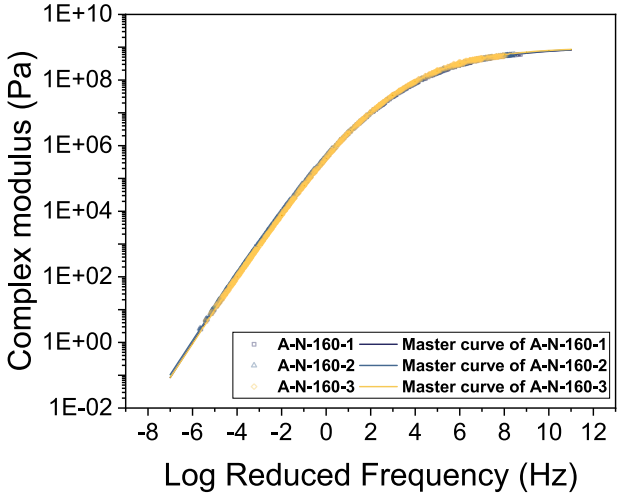

(b)

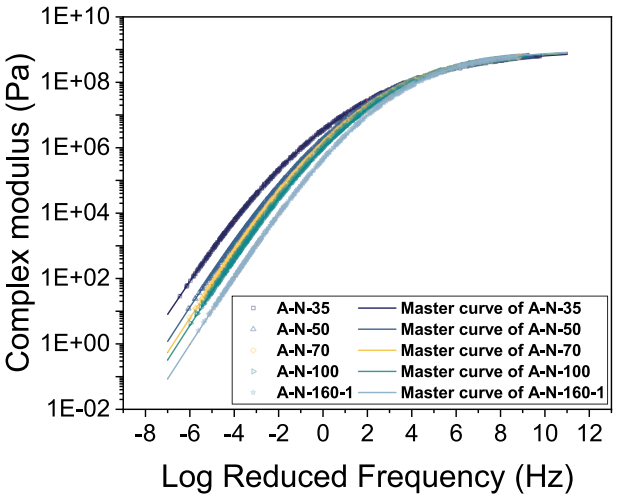

(c)

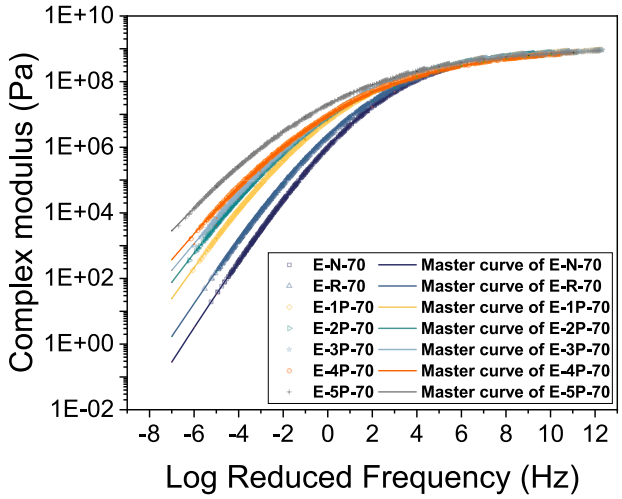

(d)

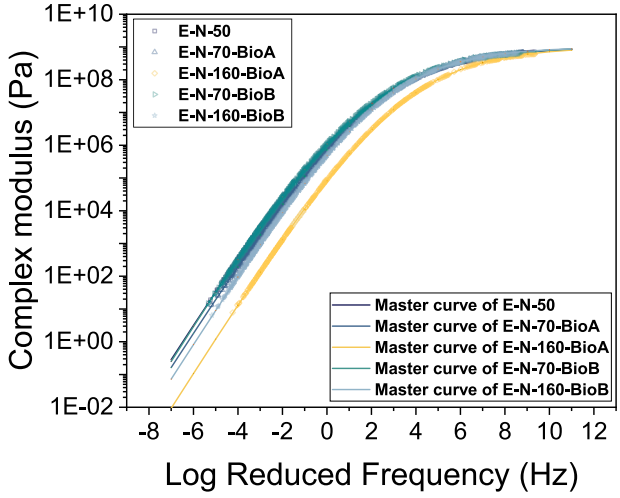

(e)

Fig. 6. Master curves of $|G^*|$ with different effects: (a) source; (b) batch; (c) penetration; (d) aging; (e) extender.

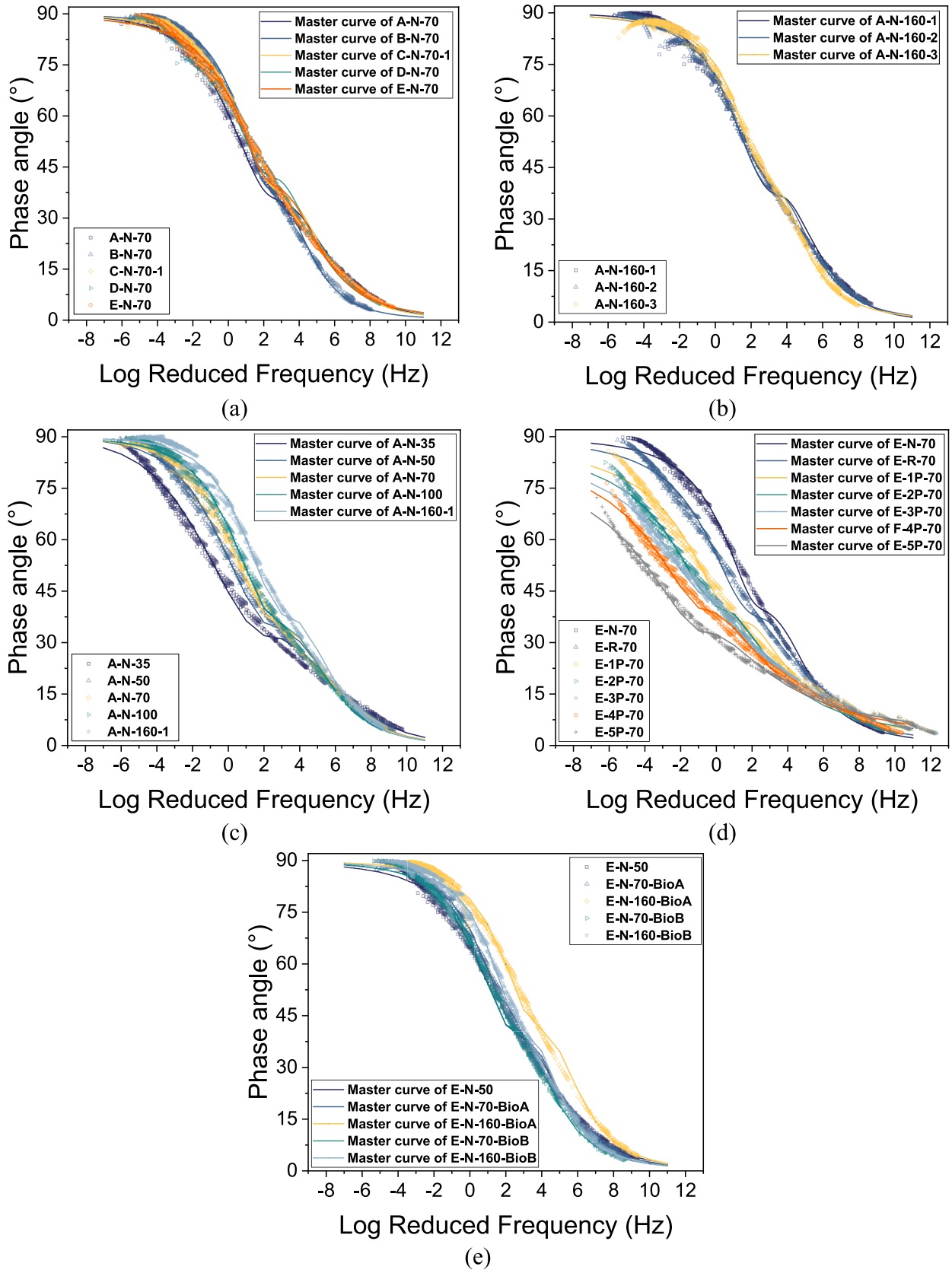

Fig. 7. Master curves of δ with different effects: (a)source; (b)batch; (c)penetration; (d)aging; (e)extender.

Table 2
The weight value of asphalt samples.

Chemical composition	W_i / % Oil source	Batch	Penetration	Aging level	Bio extender
A726	10.11	16.14	3.07	0.53	0.68
A748	14.13	11.97	8.49	1.07	8.90
A812	8.30	9.12	6.42	2.58	3.81
A864	13.32	20.18	7.88	4.02	5.27
A1030	20.25	14.18	44.31	25.61	15.16
A1378	7.99	3.18	3.62	1.48	0.90
A1460	6.56	4.54	3.21	0.90	1.27
A1600	7.75	10.09	7.86	4.30	3.52
A1700	0	0	0	58.17	57.79
A2855	6.58	7.68	6.35	0.61	1.62
A2924	5.02	2.90	8.79	0.73	1.09

based asphalt material also contain these functional groups and results in a different absorption peak at 1700 cm^{-1}.

These variations in functional groups cause bitumen to exhibit different viscoelastic responses. However, the viscoelastic response of different asphalts is consistent with changes in temperature and frequency. Both their $|G^*|$ and δ decrease and increase, respectively, with increasing temperature; and increase and decrease, respectively, with increasing frequency. The master curves of asphalt binders with different sources and batches are basically consistent with each other (Figs. 6(a) and (b) and Figs. 7(a) and (b)), suggesting a small influence of oil source and batch on the rheological properties. However, the penetration degree and aging level can cause large variations in the rheological properties of binders. Specifically, at high temperatures, binders with lower penetration have higher $|G^*|$ and lower δ show better rutting resistance (Fig. 6(c) and Fig. 7(c)). Similarly, binders with high aging levels become harder, thus also exhibiting higher $|G^*|$ and lower δ at high temperatures (Fig. 6(d) and Fig. 7(d)), resulting in better high-temperature properties. In contrast, the addition of bio-extenders can greatly improve the viscous response of binders. Bio-based binders, even at the lowest temperatures, still exhibit lower $|G^*|$ and higher δ, resulting in better low-temperature cracking resistance.

4.2. Prediction models and discussions

In this study, 25,820 observations were collected from 67 asphalt binder samples. The input data consists of 13 features, including 11 chemical properties, 1 temperature value, and 1 frequency value. The outputs represent the rheological properties, namely, the complex modulus ($|G^*|$) and phase angle (δ). The dataset was split, with 70 % randomly allocated for training and the rest 30 % reserved for testing. Model training and hyperparameter optimization were conducted using the scikit-learn and scikit-optimize packages in a Python 3.10.7 environment. All computations were performed on a workstation at Aalto University equipped with Intel Core i9-11900 CPUs and 32 GB of RAM.

As discussed, Bayesian optimization was employed for hyperparameter selection in the SVR, ANN, RF, and XGBoost models. For each combination of hyperparameters, 5-fold cross-validation (CV) was applied, with the negative coefficient of determination ($-R^2$) used as the objective function for optimization. R^2 can be calculated (see Appendix 3),

The hyperparameter ranges and the selected values for predicting $|G^*|$ and δ are summarized in Table 3. It can be observed that the tuned hyperparameter values for the $|G^*|$ and δ of the asphalt binders are nearly identical. This aligns with the fundamental principle that the rheological properties $|G^*|$ and δ are inherently correlated. The hyperparameter optimization process is carried out using Bayesian optimization. For instance, the process for optimizing the hyperparameters of XGBoost is illustrated in Fig. 8. In Fig. 8(a), the optimizer searches for the optimal hyperparameter combination that minimizes the $-R^2$ score. Here, the contour maps represent the objective function value ($-R^2$ score) being optimized. The red star in the contour maps indicates the currently known optimal solution in the hyperparameter space, which is the best hyperparameter combination found so far that minimizes the objective function. The red dotted line represents the current best-found hyperparameter value during the Bayesian optimization process. Fig. 8 (b) shows that after 10 iterations, the objective function value converges, allowing the selection of the best hyperparameter combination. In Table 3, the prefix "FT" is used to denote the optimal hyperparameters selected for each model.

To evaluate the performance of the machine learning models, in addition to R^2, four other evaluation metrics are employed: Mean Squared Error (MSE), Root Mean Squared Error (RMSE), Mean Absolute Error (MAE), and Mean Absolute Percentage Error (MAPE), see Appendix 3. Among all the evaluation metrics, R^2 provides an overall measure of the fit between the actual and predicted data, with values closer to 1.0 indicating excellent model performance. However, when the R^2 values of all models are close to 1.0, it becomes difficult to differentiate their performance. Therefore, additional metrics—MSE, RMSE, and MAE—are included in this study. MSE represents the average squared difference between real and predicted values and is particularly sensitive to outliers. RMSE and MAE measure absolute errors, with RMSE assigning greater weight to larger errors, while MAE treats all errors equally. To account for relative differences, the percentage-based error metric, MAPE, is also employed. Using multiple evaluation metrics enables a more comprehensive assessment of the performance of various machine learning models [56].

The prediction results for the complex modulus ($|G^*|$) of asphalt binders using various machine learning models are presented in Fig. 9. We can see that the predicted values for both the training and testing datasets are closely aligned across all models, indicating no significant overfitting issues. Among the models, the MLR model performs the worst, as its predicted modulus values deviate considerably from the

Table 3
Automatic hyperparameter tuning.

Model	Hyperparameters	Data type	Automatic Tuning range	Tuned value for $\|G^*\|$	Tuned value for δ
FT-SVR	Regularization parameter	Real	[$1e^{-6}$, $1e^{9}$]	967131224.9	1934.3
	Kernel coefficient	Categorical	{'scale', 'auto'}	'scale'	'scale'
	Degree of the kernel	Categorical	{1, 2, 3}	3	3
	Kernel	Categorical	{'rbf', 'linear', 'degree', 'sigmoid'}	'rbf'	'rbf'
FT-ANN	Learning rate	Categorical	{'constant', 'invscaling', 'adaptive'}	'adaptive'	'adaptive'
	Epochs	Categorical	{1000, 2000, 3000}	2000	2000
FT-RF	Number of trees	Integer	[10,2000]	2000	2000
	Maximum depth	Integer	[1,50]	32	22
	Minimum sample splits	Categorical	{2, 5, 10}	2	2
	Minimum leaf samples	Categorical	{1, 2, 4}	1	1
FT-XGBoost	Number of trees	Integer	[10, 2000]	1485	1485
	Maximum depth	Integer	[1,50]	34	34
	Maximum leaves	Integer	[1,50]	32	32
	Learning rate	Real	[0.01, 1]	0.1253	0.1253

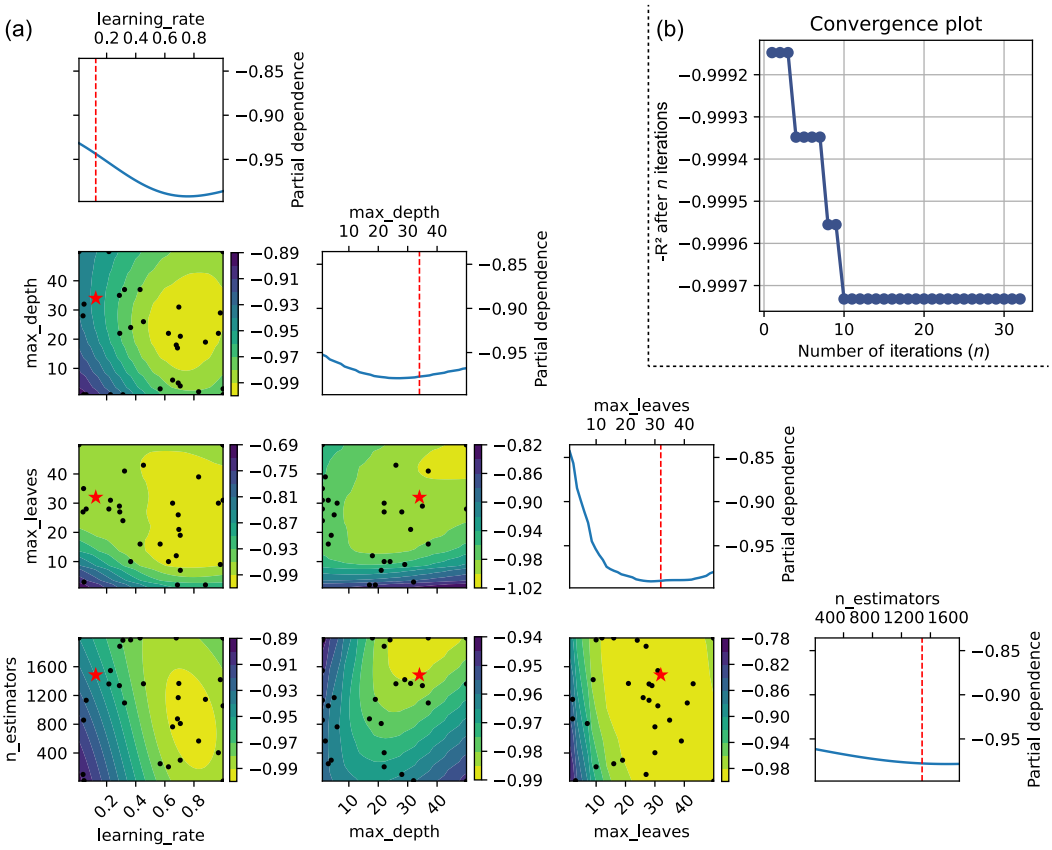

Fig. 8. Hyperparameter optimization process for the FT-XGBoost.

ground truth. In contrast, the FT-SVR and FT-ANN models achieve better performance, suggesting the presence of strong nonlinear relationships between the input features—the asphalt binders' chemical properties, frequency, and temperature—and the output. Notably, the FT-XGBoost model outperforms all other models. For R^2, it achieves an impressive value of 0.9998 on the testing dataset, which is very close to perfect prediction. Additionally, the FT-XGBoost model records the lowest RMSE value, further highlighting its superior accuracy. Following the FT-XGBoost model, the FT-RF model ranks as the second most accurate, demonstrating the effectiveness of tree-based models in predicting the binders' rheological properties using chemical features, temperature, and frequency data. When tree-based machine learning models are utilized, the prediction errors for $|G^*|$ are mostly within ± 25 %.

The prediction results for the phase angles (δ) of asphalt binders are shown in Fig. 10. When predicting phase angles, it is important to note that all predicted values are constrained within the range [0,90°]. From Fig. 10, it is evident that, similar to Fig. 9, the predictions for both the training and testing datasets are closely aligned across all five machine learning models, confirming that the models are able to generalize well to unseen data. Notably, the MLR and FT-SVR models perform better in predicting phase angles than modulus, achieving R^2 values of 0.9453 and 0.9989, respectively, on the testing datasets. Furthermore, the FT-ANN and FT-RF models show very similar performances, with R^2 values of 0.9994 and 0.9995, respectively, on the testing dataset. The FT-RF model achieves a slightly lower RMSE value of 0.6424, indicating slightly higher accuracy. Among all models, FT-XGBoost delivers the best results in terms of both R^2 and RMSE, reaffirming the effectiveness of XGBoost in addressing the proposed rheological property prediction problems.

To provide a clearer picture of the models' performance, additional evaluation metrics for the employed machine learning models are listed in Table 4. The results reveal that the MSE and MAE values decrease in the following order: MLR, FT-SVR, FT-ANN, FT-RF, and FT-XGBoost. This indicates that the predictive performance for the rheological properties of asphalt binders improves progressively in this order, with FT-XGBoost demonstrating the best capability. However, when considering the MAPE metric, the FT-RF model achieves the lowest value for predicting the modulus $|G^*|$, with FT-XGBoost as the second best. This suggests that FT-XGBoost, while superior in most metrics, exhibits a slightly higher average absolute percentage error compared to FT-RF in this specific case. For the prediction of the phase angle δ, however, FT-XGBoost consistently outperforms all other models across all indicators.

To further explore this phenomenon and explain the machine learning model's prediction results, SHapley Additive exPlanations (SHAP) values [57] were employed to evaluate the contribution of each feature in the prediction process. SHAP is a method for explaining the predictions of machine learning models, based on a game-theoretic approach that utilizes classic Shapley values from game theory and their related extensions [57]. In this approach, each feature is regarded as a "player," and its contributions to the final outcomes are quantified.

The SHAP value is additive, allowing the contribution of each feature to the output to be calculated independently and summed up. This property enables accurate and localized interpretations of a model's prediction for a specific input. SHAP values represent the difference between the expected model output and the actual output for a given input, with the contributions of all features adding up to this difference. Widely used in current machine learning model analysis, SHAP values offer meaningful and reasonable explanations for prediction results, making them a powerful tool for understanding model behavior.

The SHAP values of the FT-XGBoost model for predicting the modulus $|G^*|$ and phase angle δ in the testing dataset are shown in Fig. 11, which provides a clearer understanding of the predictive patterns. Specifically, Fig. 11(a) and 11(c) display the feature importance based on the mean absolute SHAP values, while Fig. 11(b) and 11(d)

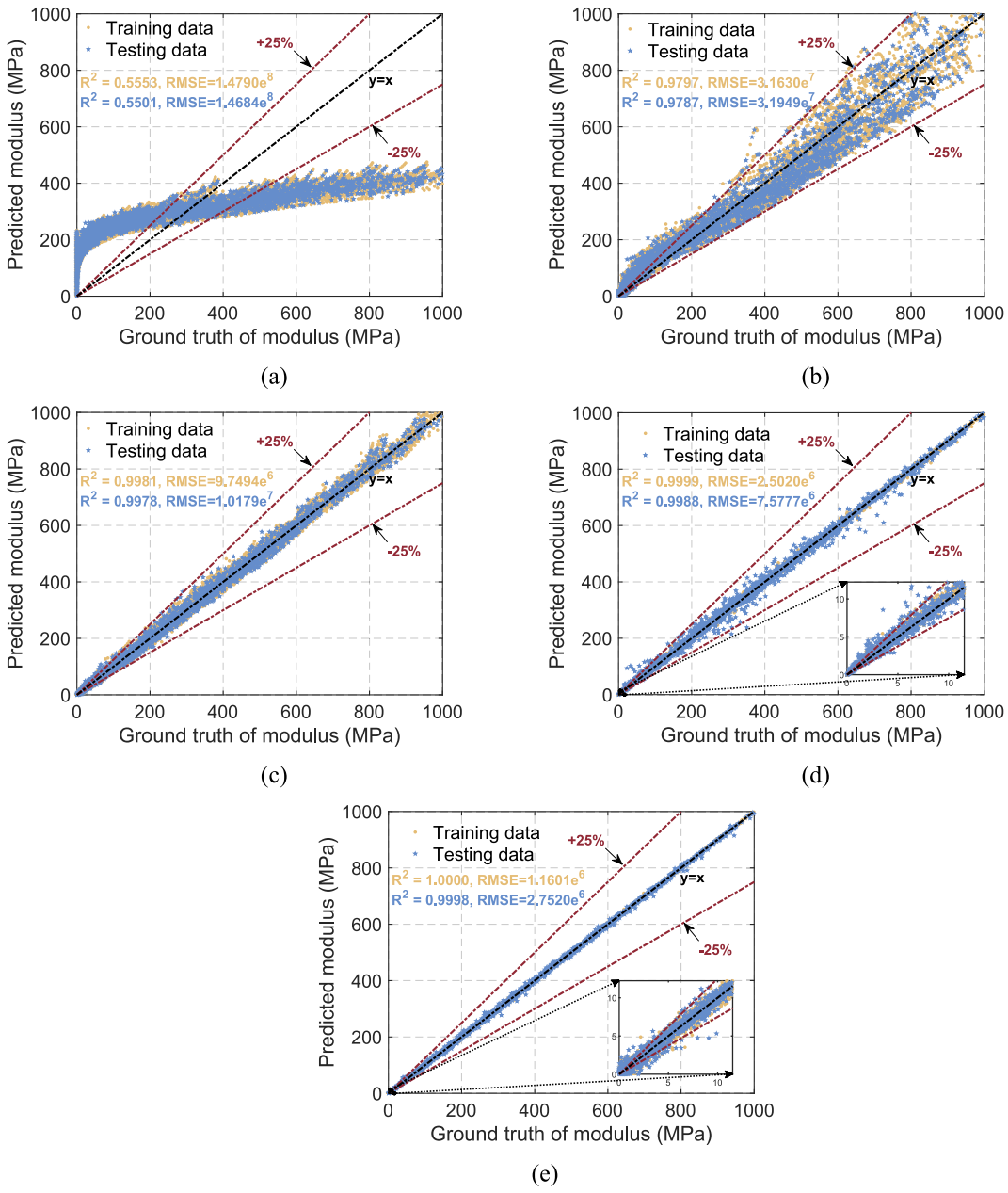

Fig. 9. Prediction results of $|G^*|$ using (a) MLR, (b) FT-SVR, (c) FT-ANN, (d) FT-RF, and (e) FT-XGBoost.

illustrate the impact of all features on the model outputs. From Fig. 11, it is evident that the top five most important features for predicting both $|G^*|$ and δ are temperature, frequency, A1030 (sulfoxide stretching), A1378 (CH_3 bending), and A1600 (C=C stretching), although the exact order of importance differs slightly between the two predictions. Beyond these five features, the contributions of other features are relatively minor, indicating that the modulus and phase angles of asphalt binders are strongly correlated and influenced by similar chemical properties. Additionally, temperature emerges as a critical factor in determining the rheological properties for both modulus and phase angles. Frequency and sulfoxide stretching have nearly identical mean impacts on the model outputs, as illustrated in Fig. 11(a) and 11(c). This analysis highlights the key role of these features in predicting the rheological properties of asphalt binders.

More specifically, from Fig. 11(b) and 11(d), for the modulus, it is clear that temperature exhibits a negative influence, indicating that higher temperatures lead to lower modulus values for asphalt binders. Additionally, frequency, sulfoxide stretching, and C=C stretching show a positive correlation with the modulus, while CH_3 bending shows a negative impact. This suggests that increasing frequency and sulfoxide stretching can enhance the modulus of the asphalt binders. For phase angles, the SHAP values of temperature are widely distributed, reflecting its varying influence across different testing samples. Unlike its role in predicting the modulus, higher temperatures and higher values of CH_3 bending are positively correlated with increased phase angles. Conversely, higher values of frequency, sulfoxide stretching, and C=C stretching result in lower phase angles. This distinction highlights the differing roles of these features in influencing the modulus and phase angles of asphalt binders.

The above analysis highlights the influence of all input features on the output of the FT-XGBoost model, emphasizing the critical role of temperature in determining the rheological properties of asphalt binders. For predicting the modulus, as shown in Fig. 9(d) and 9(e), the zoomed-in sections reveal that the FT-RF model demonstrates superior capability in predicting low modulus values of asphalt binders. While FT-XGBoost outperforms in predicting high modulus values, its

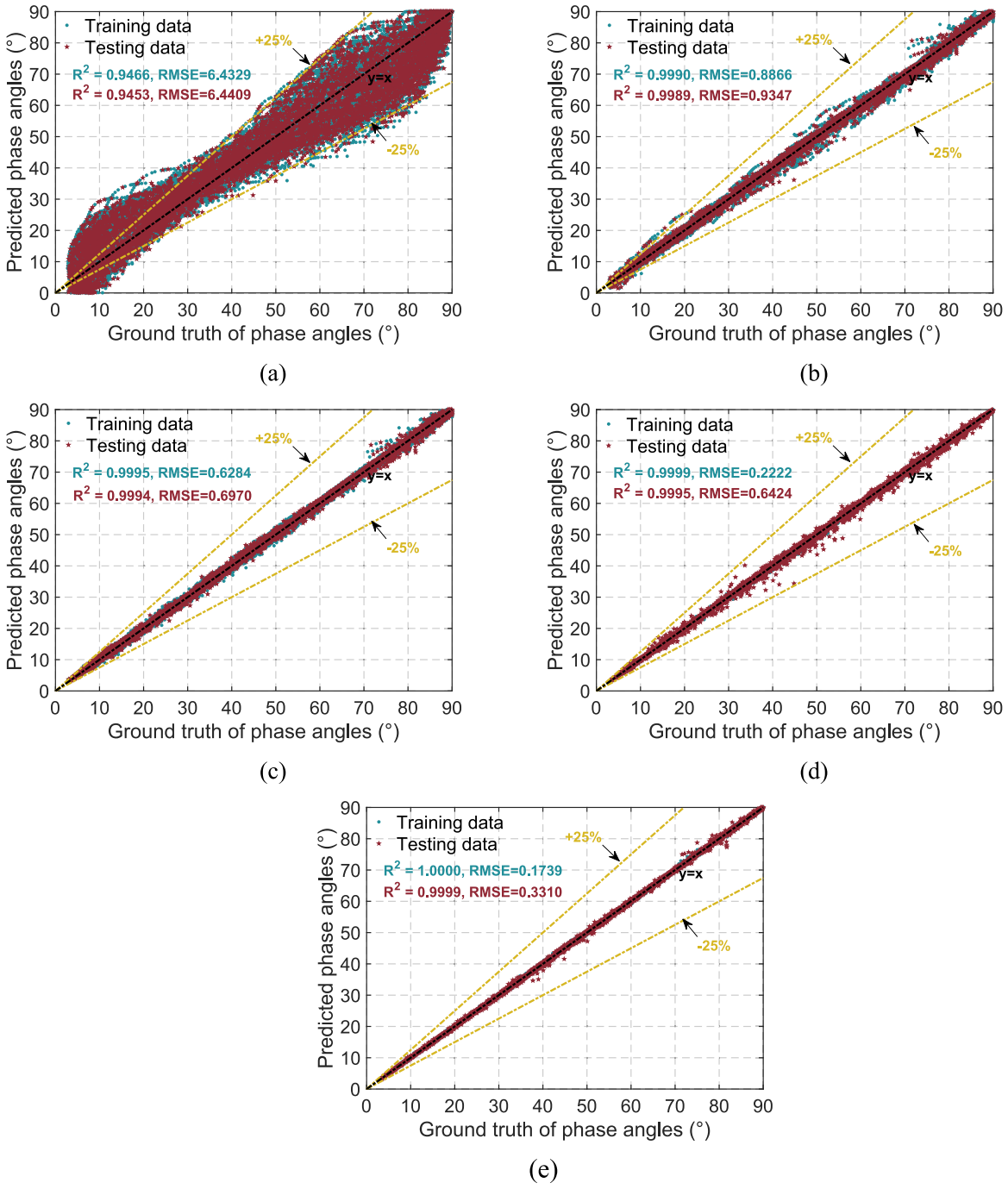

Fig. 10. Prediction results of δ using (a) MLR, (b) FT-SVR, (c) FT-ANN, (d) FT-RF, and (e) FT-XGBoost.

Table 4
Different indicators on model performance.

Models	Indicators for predicting $\|G^*\|$			Indicators for predicting δ		
	MSE	MAE	MAPE (%)	MSE	MAE	MAPE (%)
MLR	$2.16e^{16}$	$1.18e^{8}$	$2.07e^{7}$	41.49	4.98	19.72
FT-SVR	$1.02e^{15}$	$1.73e^{7}$	$1.87e^{5}$	0.87	0.61	2.41
FT-ANN	$1.04e^{14}$	$5.04e^{6}$	$1.46e^{4}$	0.49	0.51	1.77
FT-RF	$5.74e^{13}$	$2.97e^{6}$	14.22	0.41	0.39	1.19
FT-XGboost	$7.57e^{12}$	$1.32e^{6}$	$1.25e^{4}$	0.11	0.22	0.66

relatively poorer predictions for low modulus contribute to a higher MAPE indicator. From the SHAP value analysis, it is clear that temperature has the most significant influence on predictions. Therefore, to leverage the strengths of both the FT-RF and FT-XGBoost models, the original dataset was split into two subsets based on a threshold of 22 °C: Dataset 1 (temperature range of [-30, 22)) and Dataset 2 (temperature range of [22, 76]). The FT-XGBoost model was applied to Dataset 1, while FT-RF was used for Dataset 2. After computation, the combination of FT-RF and FT-XGBoost models achieves the following indicators on the original dataset: $R^2 = 0.9999$, MSE = $6.94e^{12}$, RMSE = $2.64e^{6}$, MAE = $1.21e^{6}$, and MAPE = 14.19 %. These indicators outperform those of the individual FT-RF or FT-XGBoost models, as indicated in Fig. 9 and Table 4, demonstrating the effectiveness of this model combination strategy in improving modulus prediction accuracy and robustness across different temperature ranges.

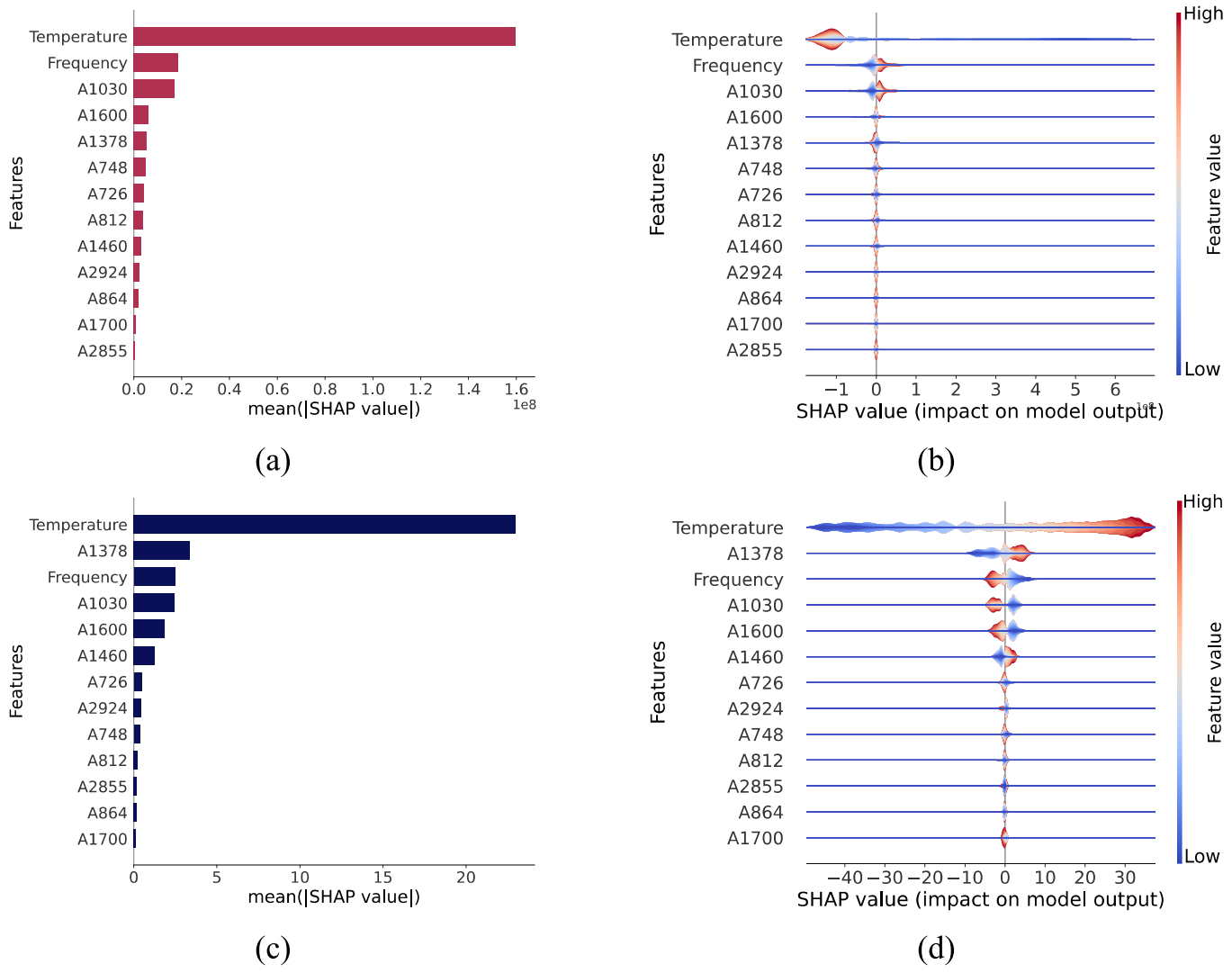

Fig. 11. SHAP values of FT-XGBoost model prediction: (a) mean of absolute SHAP values for predicting |G*|, (b) SHAP values for predicting |G*|, (c) mean of absolute SHAP values for predicting δ, (d) SHAP values for predicting δ.

5. Conclusions

This study investigated the relationship between the rheological properties and chemical composition of asphalt binders based on laboratory tests and five machine learning algorithms, with Bayesian optimization used to determine optimal hyperparameters and maximize model performance. Results show a strong correlation between chemical composition and rheological properties, and FT-XGBoost can well predict the modulus ($|G^*|$) and phase angle (δ) of binders. The specific findings of the study are as follows:

The chemical compositions of asphalt binders are not sensitive to variations in oil source and production batch, with the maximum weight of their coefficient of variation being around 20 %. This makes it challenging to establish a direct relationship between chemical composition and rheological properties. However, the chemical compositions of asphalt binders are sensitive to penetration, aging level, and bio-extender, as reflected in the vibrations of functional groups such as S=O, C=O, and C-O-C. The strong correlation between changes in these functional groups and the $|G^*|$ and δ underscores the potential for predictive modeling.

The trained FT-XGBoost model outperforms MLR, FT-SVR, FT-ANN, and FT-RF in predicting the $|G^*|$ and δ of asphalt binders. Using chemical compositions along with frequency and temperature, it achieves R^2 values of 0.9998 and 0.9999 for $|G^*|$ and δ, respectively. SHAP values indicate that temperature, frequency, and functional groups A1030 (sulfoxide stretching), A1378 (CH_3 bending), and A1600 (C=C stretching) are the five most important factors for predicting both $|G^*|$ and δ, further confirming the strong correlations between these variables. Temperature is identified as a critical influencing factor. To further improve predictive performance, it is recommended to use FT-XGBoost for low temperatures ([−30 °C, 22 °C)) and FT-RF for high temperatures ([22 °C, 76 °C]).

CRediT authorship contribution statement

Fan Zhang: Writing – review & editing, Writing – original draft, Validation, Methodology, Investigation, Funding acquisition, Formal analysis, Data curation. **Augusto Cannone Falchetto:** Writing – review & editing, Supervision, Funding acquisition. **Di Wang:** Writing – review & editing, Methodology, Investigation, Data curation. **Zhenkun Li:** Writing – review & editing, Writing – original draft, Validation, Methodology, Formal analysis. **Yuxuan Sun:** Methodology, Investigation, Data curation. **Weiwei Lin:** Writing – review & editing, Supervision.

Declaration of competing interest

The authors declare that they have no known competing financial interests or personal relationships that could have appeared to influence the work reported in this paper.

Acknowledgment

This work was funded by the MoreBit project from the Finnish Transport Infrastructure Agency and Industries. Fan Zhang acknowledges the support from the National & Local Joint Engineering Research Center of Transportation and Civil Engineering Materials, Chongqing Jiaotong University (grant number: TCEM-2023-02) and the Finnish Section of the Nordic Road Association (PTL ry). Weiwei Lin and Zhenkun Li acknowledge the support from Aalto University (research project funding in ENG 2022). Yuxuan Sun acknowledges the China Scholarship Council for the financial support for pursuing a PhD degree (Grant number: 2024407960006).

Appendix 1. Description of asphalt binder samples

Number	Source	Batch	Grade	Aging level	Bio type	Sample name
1	A	–	35/50	Neat	–	A-N-35
2	A	–	50/70	Neat	–	A-N-50
3	A	–	70/100	Neat	–	A-N-70
4	A	–	100/120	Neat	–	A-N-100
5	A	1	160/220	Neat	–	A-N-160-1
6	A	2	160/220	Neat	–	A-N-160-2
7	A	3	160/220	Neat	–	A-N-160-3
8	B	–	70/100	Neat	–	B-N-70
9	B	–	100/120	Neat	–	B-N-100
10	B	1	160/220	Neat	–	B-N-160-1
11	B	2	160/220	Neat	–	B-N-160-2
12	C	1	70/100	Neat	–	C-N-70-1
13	C	2	70/100	Neat	–	C-N-70-2
14	C	–	100/120	Neat	–	C-N-100
15	C	–	120/150	Neat	–	C-N-120
16	C	1	160/220	Neat	–	C-N-160-1
17	C	2	160/220	Neat	–	C-N-160-2
18	D	–	70/100	Neat	–	D-N-70
19	E	–	50/70	Neat	–	E-N-50
20	E	–	70/100	Neat	–	E-N-70
21	E	–	100/160	Neat	–	E-N-160
22	E	–	70/100	Neat	A	E-N-70-BioA
23	E	–	100/160	Neat	A	E-N-160-BioA
24	E	–	70/100	Neat	B	E-N-70-BioB
25	E	–	100/160	Neat	B	E-N-160-BioB
26	E	–	50/70	Short-term aged	–	E-R-50
27	E	–	70/100	Short-term aged	–	E-R-70
28	E	–	100/160	Short-term aged	–	E-R-160
29	E	–	70/100	Short-term aged	A	E-R-70-BioA
30	E	–	100/160	Short-term aged	A	E-R-160-BioA
31	E	–	70/100	Short-term aged	B	E-R-70-BioB
32	E	–	100/160	Short-term aged	B	E-R-160-BioB
33	E	–	50/70	Long-term aged	–	E-1P-50
34	E	–	70/100	Long-term aged	–	E-1P-70
35	E	–	100/160	Long-term aged	–	E-1P-160
36	E	–	70/100	Long-term aged	A	E-1P-70-BioA
37	E	–	100/160	Long-term aged	A	E-1P-160-BioA
38	E	–	70/100	Long-term aged	B	E-1P-70-BioB
39	E	–	100/160	Long-term aged	B	E-1P-160-BioB
40	E	–	50/70	Long-term aged	–	E-2P-50
41	E	–	70/100	Extended long-term aged (2PAV)	–	E-2P-70
42	E	–	100/160	Extended long-term aged (2PAV)	–	E-2P-160
43	E	–	70/100	Extended long-term aged (2PAV)	A	E-2P-70-BioA
44	E	–	100/160	Extended long-term aged (2PAV)	A	E-2P-160-BioA
45	E	–	70/100	Extended long-term aged (2PAV)	B	E-2P-70-BioB
46	E	–	100/160	Extended long-term aged (2PAV)	B	E-2P-160-BioB
47	E	–	50/70	Extended long-term aged (3PAV)	–	E-3P-50
48	E	–	70/100	Extended long-term aged (3PAV)	–	E-3P-70
49	E	–	100/160	Extended long-term aged (3PAV)	–	E-3P-160
50	E	–	70/100	Extended long-term aged (3PAV)	A	E-3P-70-BioA
51	E	–	100/160	Extended long-term aged (3PAV)	A	E-3P-160-BioA
52	E	–	70/100	Extended long-term aged (3PAV)	B	E-3P-70-BioB
53	E	–	100/160	Extended long-term aged (3PAV)	B	E-3P-160-BioB
54	E	–	50/70	Extended long-term aged (4PAV)	–	E-4P-50
55	E	–	70/100	Extended long-term aged (4PAV)	–	E-4P-70
56	E	–	100/160	Extended long-term aged (4PAV)	–	E-4P-160
57	E	–	70/100	Extended long-term aged (4PAV)	A	E-4P-70-BioA
58	E	–	100/160	Extended long-term aged (4PAV)	A	E-4P-160-BioA
59	E	–	70/100	Extended long-term aged (4PAV)	B	E-4P-70-BioB
60	E	–	100/160	Extended long-term aged (4PAV)	B	E-4P-160-BioB

(*continued on next page*)

(*continued*)

Number	Source	Batch	Grade	Aging level	Bio type	Sample name
61	E	–	50/70	Extended long-term aged (5PAV)	–	E-5P-50
62	E	–	70/100	Extended long-term aged (5PAV)	–	E-5P-70
63	E	–	100/160	Extended long-term aged (5PAV)	–	E-5P-160
64	E	–	70/100	Extended long-term aged (5PAV)	A	E-5P-70-BioA
65	E	–	100/160	Extended long-term aged (5PAV)	A	E-5P-160-BioA
66	E	–	70/100	Extended long-term aged (5PAV)	B	E-5P-70-BioB
67	E	–	100/160	Extended long-term aged (5PAV)	B	E-5P-160-BioB

Appendix 2. Calculation of weight value

$$V_i = \frac{\sigma_i}{X_i} \text{(A.2.1)}$$

$$W_i = \frac{V_i}{\sum_{i=1}^{n} V_i} \text{(A.2.2)}$$

where, V_i is the coefficient of variation; σ_i is the standard deviation; X_i is the average value; W_i is the weight value.

Appendix 3. Calculation of R^2, MSE, RMSE, MAE, and MAPE

$$R^2 = 1 - \frac{\sum_{i=1}^{N}\left(y_i - \widehat{y_i}\right)^2}{\sum_{i=1}^{N}\left(y_i - \bar{y}\right)^2} \text{(A.3.1)}$$

$$MSE = \frac{1}{N}\sum_{i=1}^{N}\left(y_i - \widehat{y}_i\right)^2 \text{(A.3.2)}$$

$$RMSE = \sqrt{\frac{1}{N}\sum_{i=1}^{N}\left(y_i - \widehat{y}_i\right)^2} \text{(A.3.3)}$$

$$MAE = \frac{1}{N}\sum_{i=1}^{N}\left|y_i - \widehat{y}_i\right| \text{(A.3.4)}$$

$$MAPE = \left(\frac{1}{N}\sum_{i=1}^{N}\left|\frac{y_i - \widehat{y_i}}{y_i}\right|\right)\cdot 100\% \text{(A.3.5)}$$

where y_i represents the ground-truth values, $\hat{y}_i$ represents the predicted values, and $\bar{y}$ represents the average of the true values, calculated as $\frac{1}{N}\sum_{i=1}^{N} y_i$.

Data availability

Data will be made available on request.

References

[1] Zhou L, Airey G, Zhang Y, Huang W, Wang C. A novel fatigue test method for bitumen-stone combinations under cyclic tension-compression loading. Mater Des 2025;249:113577.

[2] Zhou L, Huang W, Zhang Y, Lv Q, Yan C, Jiao Y. Evaluation of the adhesion and healing properties of modified asphalt binders. Constr Build Mater 2020;251:119026.

[3] Zhang F, Falchetto AC, Yuan D, Wang W, Wang D, Sun Y. Research on performance variations of different asphalt binders results from microwave heating during freeze-thaw cycles. Constr Build Mater 2024;448:138280.

[4] Sun Y, Li H, Yang B, Han Y, Zou Z. Investigation on rheological properties and aging mechanism of asphalt under multiple environmental conditions. Constr Build Mater 2024;443:137713.

[5] Anderson DA, Christensen DW, Bahia HU, Dongre R, Sharma M, Antle CE, Button J. Binder characterization and evaluation, volume 3: Physical characterization. Strategic Highway Research Program, National Research Council, Washington, DC; 1994.

[6] Osman H, Rodzey MZIM, Hasan MRM, Wong TLX, Ghazali MFHM, Zakaria Z, et al. Review of bonding behavior, mechanisms, and characterization approach in bituminous materials under different conditions. J Traffic Transp Eng (English Edition) 2024.

[7] Xu J, Wang Z, Fan Z, Liu J, Lu G, Wang D. Nonlinear rheological behavior of asphalt based on large amplitude oscillation shear test under different loading, aging, and modification conditions. J Road Eng 2025.

[8] Liu F, Wen H. Prediction of rheological and damage properties of asphalt binders that result from oxidative aging. Transp Res Rec 2015;2505(1):92–8.

[9] Shan L, Wang Y, Liu S, Qi X, Wang J. Establishment of correlation model between compositions and dynamic viscoelastic properties of asphalt binder based on machine learning. Constr Build Mater 2023;364:129902.

[10] Nivitha M, Ma J, Hesp SA. Effect of model compounds on stress relaxation in asphalt binders. Constr Build Mater 2024;457:139347.

[11] Sultana S, Bhasin A. Effect of chemical composition on rheology and mechanical properties of asphalt binder. Constr Build Mater 2014;72:293–300.

[12] Cao Y, Li J, Liu Z, Li X, Zhang F, Shan B. Rheological properties of styrene-butadiene-styrene asphalt mastic containing high elastic polymer and snow melting salt. Polymers 2022;14(17):3651.

[13] Michalica P, Kazatchkov IB, Stastna J, Zanzotto L. Relationship between chemical and rheological properties of two asphalts of different origins. Fuel 2008;87(15–16):3247–53.

[14] Zhang F, Sha A, Cao Y, Wang W, Song R, Jiao W. Characterization of self-healing properties of asphalt pavement materials containing carbon nanotubes: from the binder and mix level based on grey relational analysis. Constr Build Mater 2023;404:133323.

[15] Li Z, Lan Y, Lin W. Footbridge damage detection using smartphone-recorded responses of micromobility and convolutional neural networks. Autom Constr 2024;166:105587.

[16] Li Z, Lan Y, Lin W. Indirect frequency identification of footbridges with pedestrians using the contact-point response of shared scooters. J Bridg Eng 2024;29(6):04024036.

[17] Yang X, Zhang J, Liu W, Jing J, Zheng H, Xu W, et al. Automation in road distress detection, diagnosis and treatment. J Road Eng 2024;4(1):1–26.

[18] Han Z, Tang J, Hu L, Jiang W, Sha A. Automated measurement of asphalt pavement rut depth using smartphone imaging. Autom Constr 2025;174:106124.

[19] Goldstein BA, Navar AM, Carter RE. Moving beyond regression techniques in cardiovascular risk prediction: applying machine learning to address analytic challenges. Eur Heart J 2017;38(23):1805–14.

[20] Jamshidi A, Pelletier J-P, Martel-Pelletier J. Machine-learning-based patient-specific prediction models for knee osteoarthritis. Nat Rev Rheumatol 2019;15(1):49–60.

[21] Marcelino P, de Lurdes Antunes M, Fortunato E, Gomes MC. Machine learning approach for pavement performance prediction. Int J Pavement Eng 2021;22(3):341–54.

[22] Alnaqbi AJ, Zeiada W, Al-Khateeb G, Abttan A, Abuzwidah M. Predictive models for flexible pavement fatigue cracking based on machine learning. Transp Eng 2024;16:100243.

[23] Hosseini AS, Hajikarimi P, Gandomi M, Nejad FM, Gandomi AH. Optimized machine learning approaches for the prediction of viscoelastic behavior of modified asphalt binders. Constr Build Mater 2021;299:124264.

[24] Ziari H, Amini A, Goli A, Mirzaiyan D. Predicting rutting performance of carbon nano tube (CNT) asphalt binders using regression models and neural networks. Constr Build Mater 2018;160:415–26.

[25] Arifuzzaman M, Gazder U, Islam MS, Mamun AA. Prediction and sensitivity analysis of CNTs-modified asphalt's adhesion force using a radial basis neural network model. J Adhes Sci Technol 2020;34(10):1100–14.

[26] Tarefder R, Ahsan S. Neural network modelling of asphalt adhesion determined by AFM. J Microsc 2014;254(1):31–41.

[27] AASHTO-T240, Standard Method of Test for Effect of Heat and Air on a Moving Film of Asphalt Binder (Rolling Thin-Film Oven Test), American Association of State Highway and Transportation Officials, Washington, DC, USA, 2013.

[28] AASHTO-R28-12, Standard Practice for Accelerated Aging of Asphalt Binder Using a Pressurized Aging Vessel (PAV), American Association of State Highway and Transportation Officials, Washington, DC, USA, 2012.
[29] Goldenstein CS, Spearrin RM, Jeffries JB, Hanson RK. Infrared laser-absorption sensing for combustion gases. Prog Energy Combust Sci 2017;60:132–76.
[30] Hou X, Lv S, Chen Z, Xiao F. Applications of Fourier transform infrared spectroscopy technologies on asphalt materials. Measurement 2018;121:304–16.
[31] Yang X, You Z, Mills-Beale J. Asphalt binders blended with a high percentage of biobinders: Aging mechanism using FTIR and rheology. J Mater Civ Eng 2015;27 (4):04014157.
[32] Ding H, Hesp SA. Variable-temperature Fourier-transform infrared spectroscopy study of asphalt binders from the SHRP Materials Reference Library. Fuel 2021; 298:120819.
[33] Ma L, Varveri A, Jing R, Erkens S. Chemical characterisation of bitumen type and ageing state based on FTIR spectroscopy and discriminant analysis integrated with variable selection methods. Road Mater Pavement Des 2023;24(sup1):506–20.
[34] Weigel S, Stephan D. The prediction of bitumen properties based on FTIR and multivariate analysis methods. Fuel 2017;208:655–61.
[35] AASHTO-T315, Standard Method of Test for Determining the Rheological Properties of Asphalt Binder Using a Dynamic Shear Rheometer (DSR), American Association of State Highway and Transportation Officials, Washington, DC, USA, 2012.
[36] Khabaz F, Khare R. Molecular simulations of asphalt rheology: Application of time–temperature superposition principle. J Rheol 2018;62(4):941–54.
[37] Wang D, Baliello A, Poulikakos L, Vasconcelos K, Kakar MR, Giancontieri G, et al. Rheological properties of asphalt binder modified with waste polyethylene: An interlaboratory research from the RILEM TC WMR. Resour Conserv Recycl 2022; 186:106564.
[38] Shi K, Ma F, Fu Z, Lou B, Barbieri DM, Li J, et al. Comprehensive evaluation of sulfur content and curing duration effects on the rheological performance of sulfur-extended bitumen. Fuel 2025;393:134979.
[39] Williams ML, Landel RF, Ferry JD. The temperature dependence of relaxation mechanisms in amorphous polymers and other glass-forming liquids. J Am Chem Soc 1955;77(14):3701–7.
[40] Uyanık GK, Güler N. A study on multiple linear regression analysis. Procedia Soc Behav Sci 2013;106:234–40.
[41] Smola AJ, Schölkopf B. A tutorial on support vector regression. Stat Comput 2004; 14:199–222.
[42] Kiranyaz S, Avci O, Abdeljaber O, Ince T, Gabbouj M, Inman DJ. 1D convolutional neural networks and applications: A survey. Mech Syst Sig Process 2021;151: 107398.
[43] Breiman L. Random forests Machine learning 2001;45:5–32.
[44] Chen T, Xgboost GC. A scalable tree boosting system. In: Proceedings of the 22nd acm sigkdd international conference on knowledge discovery and data mining; 2016. p. 785–94.
[45] Wang X, Banthia N, Yoo DY. Reinforcement bond performance in 3D concrete printing: Explainable ensemble learning augmented by deep generative adversarial networks. Autom Constr 2024;158:105164.
[46] Victoria AH, Maragatham G. Automatic tuning of hyperparameters using Bayesian optimization. Evol Syst 2021;12(1):217–23.
[47] Tucker C, Newcomb W, Los S, Prince S. Mean and inter-year variation of growing-season normalized difference vegetation index for the Sahel 1981-1989. Int J Remote Sens 1991;12(6):1133–5.
[48] Milich L, Weiss E. GAC NDVI interannual coefficient of variation (CoV) images: ground truth sampling of the Sahel along north-south transects. Int J Remote Sens 2000;21(2):235–60.
[49] Jiang W, Yuan D, Tong Z, Sha A, Xiao J, Jia M, et al. Aging effects on rheological properties of high viscosity modified asphalt. J Traffic Transp Eng 2023;10(2): 304–19.
[50] Wang T, Riccardi C, Jiang W. From waste to sustainable pavement: Rejuvenation of asphalt binder using waste engine oil residue and crumb rubber. Chem Eng J 2025; 505:159523.
[51] Marsac P, Piérard N, Porot L, Van den Bergh W, Grenfell J, Mouillet V, et al. Potential and limits of FTIR methods for reclaimed asphalt characterisation. Mater Struct 2014;47:1273–86.
[52] Zhang F, Zhu J, Sun Y, Benny CM, Wang D, Cannone Falchetto A. Effect analysis of using tall oil pitch (TOP) to partially extend bitumen in asphalt pavements: comparison of different TOPs. Road Mater Pavment Des 2025. In press:1–20.
[53] Yang X, Mills-Beale J, You Z. Chemical characterization and oxidative aging of bio-asphalt and its compatibility with petroleum asphalt. J Clean Prod 2017;142: 1837–47.
[54] Qin Y, Dong R, Li Y. Characterization of light components in rubber-oil mixtures reclaimed asphalt and their effect on the self-healing performance of asphalt. Constr Build Mater 2024;444:137866.
[55] Zhao K, Wang Y, Li F. Influence of ageing conditions on the chemical property changes of asphalt binders. Road Mater Pavement Des 2021;22(3):653–81.
[56] Naser M, Alavi A. Insights into performance fitness and error metrics for machine learning. arXiv preprint arXiv:2006.00887; 2020.
[57] Lundberg S. A unified approach to interpreting model predictions. arXiv preprint arXiv:1705.07874; 2017.